Hydrothermal dolomitization of basinal deposits controlled by a synsedimentary fault system in Triassic extensional setting, Hungary

Kinga Hips, János Haas, Orsolya Győri

MTA–ELTE Geological, Geophysical and Space Science Research Group, Pázmány s. 1/c, 1117 Budapest, Hungary (hips@caesar.elte.hu)

Abstract

Dolomitization of relatively thick carbonate successions occurs via an effective fluid circulation mechanism, since the replacement process requires a large amount of Mg-rich fluid interacting with the $CaCO_3$ precursor. In the western end of the Neotethys, fault-controlled extensional basins developed during the Late Triassic spreading stage. In the Buda Hills and Danube-East blocks, distinct parts of silica and organic matter-rich slope and basinal deposits are dolomitized. Petrographic, geochemical, and fluid inclusion data distinguished two dolomite types: (1) finely to medium crystalline and (2) medium to coarsely crystalline. They commonly co-occur and show a gradual transition. Both exhibit breccia fabric under microscope. Dolomite texture reveals that the breccia fabric is not inherited from the precursor carbonates but was formed during the dolomitization process and under the influence of repeated seismic shocks. Dolomitization within the slope and basinal succession as well as within the breccia zones of the underlying basement block is interpreted as being related to fluid originated from the detachment zone and channelled along synsedimentary normal faults. The proposed conceptual model of dolomitization suggests that pervasive dolomitization occurred not only within and near the fault zones. Permeable beds have channelled the fluid towards the basin centre where the fluid was capable of partial dolomitization. The fluid inclusion data, compared with vitrinite reflectance and maturation data of organic matter, suggest that the ascending fluid was likely hydrothermal which cooled down via mixing with marine-derived pore fluid. Thermal gradient is considered as a potential driving force for fluid flow.

Keywords Cherty dolomite; Extensional basins; Hydrothermal fluid; Multiphase breccia fabric.

Introduction

Dolomitization is a replacement process which requires a large amount of Mg-rich fluid interacting with a $CaCO_3$ precursor (Land 1985; Morrow 1990). Dolomitization models are essentially based on the hydrological drive of a large-scale fluid circulation in those settings, where the deposits have been removed from the shallow burial realm, and thus, the pore fluid chemistry is no longer governed by surface processes (Machel 2004). Cherty dolomite within an organic matter-rich basinal succession had already been noticed by Hofmann (1871) from the hills surrounding Budapest. A sedimentary architecture including a carbonate platform, foreslope, and basin was reconstructed by systematic studies of the Upper Triassic formations of the region (Kleb et al. 1993; Haas 1994, 2002; Haas et al. 1997a; 2000). Although various hypotheses were proposed to explain the dolomitization process of basinal deposits (Haas et al. 1997b; Haas 2002; Esteban et al. 2009), the controlling factors were still not fully understood.

Structurally controlled hydrothermal dolomite reservoirs are considered as important hydrocarbon plays, and accordingly, they receive an increased exploration attention globally (e.g. Smith Jr. and Davies 2006). Hydrothermal dolomitization is defined as an alteration by fluid with a temperature higher than the ambient temperature of the host formation (Qing and Mountjoy 1992, 1994; Machel and Lonnee 2002). This process usually occurs at intermediate burial depths (e.g. Davies and Smith Jr 2006; Smith Jr. and Davies 2006; Wilson et al. 2007; Conlife et al. 2010; Lavoie and Chi 2010; Ronchi et al. 2012; Haeri-Ardakani et al. 2013). Fault-related hydrothermal dolomitization in compressional setting was described from several locations (e.g. Oliver 1986; summary in Machel 2004). This paper documents a peculiar breccia fabric within dolomitized organic matter-rich successions, deposited in intraplatform extensional basins. The observed features propose a dolomitization process in a tectonically active, hydrothermal fluid-dominated environment located at intermediate burial depth.

Geological setting

Mesozoic and Paleogene rocks crop out on the western and eastern side of the Danube River near Budapest, in the Buda Hills and Danube-East blocks (Fig. 1). In both areas, the Upper Triassic slope and basinal deposits overlie Middle Triassic platform dolomite; they are typified by cherty dolomite in the lower part of the succession and toe-of-slope and basinal cherty limestone upsection (Mátyáshegy Formation in the Buda Hills and Csővár Formation in the Danube-East blocks, respectively; Haas 1994, 2002; Haas et al. 1997a; Fig. 2). The cherty carbonate succession crops out in two ranges in the Buda Hills. Both dolomite and limestone occur in the eastern range where the estimated thickness of the succession is 200–250 m. Only dolomite is known in the western range where a reliable estimate of the thickness is not possible. In the Danube-East blocks, the thickness of the cherty dolomite is ca. 100 m and that of the overlying limestone is 600 m. The pervasively dolomitized deposits are poor in fossils. Based on radiolarians and conodonts, the dolomite is assigned to the Carnian–Norian interval in the Buda Hills (Kozur and Mock 1991; Haas et al. 2000). The limestone and the slightly dolomitized limestone are rich in fossils. Both pelagic elements, i.e. prasinophyte algal cysts, radiolarians, ammonites, crinoids, and conodonts, and redeposited bioclasts of shallow platform origin, i.e. calcareous algae, foraminifers, calcareous sponges, gastropods, bryozoans, corals, and holothurian sclerites, were found (Haas 1994; Haas et al. 2000). Based on these fossils, the following ages are defined for the limestone: Early Carnian limestone crops out in the north-eastern part of the Buda Hills; Late Norian–Rhaetian cherty limestone is developed in the eastern range of the Buda Hills; and Early Norian–Lower Jurassic cherty limestone occurs in the Danube-East blocks (Kozur and Mostler 1973, Detre et al. 1988; Kozur and Mock 1991; Haas et al. 2000; Karádi and Kozur 2013). Similar Upper Triassic dolomitized slope and basinal successions were described as Forni Dolomite and Bača Dolomite in the Southern Alps (Rožič et al. 2009; Gale 2010).

A thick succession of Middle Triassic platform dolomite occurs in both studied areas (Oravecz 1963; Hips et al. 2015). There is commonly a sharp boundary between the two dolomite formations but gradual transition was also recognized, where the cherty dolomite is in a higher position (Benkő and Fodor 2002).

The dolomite rocks in both study areas were subjected to moderate deformation during the Cretaceous–Early Eocene (Fodor et al. 1994, 1999; Haas et al. 1997b; Benkő and Fodor 2002). Due to tectonically induced uplift and intense denudation in the Late Cretaceous to Early Palaeogene, post-Triassic Mesozoic strata are absent in the Buda Hills, and post-Early Jurassic formations were preserved only in thin tectonic slices in the Danube-East blocks. A long erosional period was followed by deposition of bauxite, coal, and limestone in the Eocene, and marl in the Oligocene (Wein 1977; Báldi 1986). Calcite, barite, fluorite, and associated sulphide minerals were precipitated along fractures in the dolomite from hydrothermal fluid migrated along Middle Miocene fault zones (Győri et al. 2011; Poros et al. 2012). Inversion of the Neogene Pannonian Basin began in the latest Miocene and resulted in the uplift of Mesozoic–Palaeogene basement blocks.

Vitrinite reflectance (VR), as an organic maturation indicator, has become one of the main tools for thermal history analysis of sedimentary basins, since it shows strong correlation with maximum burial temperature (Baker and Pawlewitz 1986). The measured mean VR value of the limestone succession, overlying the dolomite studied, is 0.34 % in both studied areas (Hámor-Vidó et al. 1998; Haas et al. 2000; Sasvári 2009). In the Buda Hills, Hetényi et al. (2004) studied the composition of organic matter both in the dolomite and in the overlying limestone. The organic matter had accumulated during deposition and was preserved in place. The organic matter content of the deposits is relatively high; the TOC ranges from 1 to 4 %. Immaturity of organic matter is constrained by Rock–Eval data and biological marker isomerization ratios. T_{max} values measured by Rock–Eval pyrolysis range between 416 and 425 °C. The maturity of the organic matter in the dolomite interval has been found slightly higher than that of the limestone one (the comparison is based on the configurational isomerization ratios, calculated from GC/MS fragmentograms of the non-aromatic hydrocarbon fraction of bitumens; Hetényi et al. 2004). Both VR and T_{max} values indicate that organic matter maturity did not reach the temperature threshold of the onset of oil generation.

Material and methods

Two borehole cores and six outcrop sections were studied and sampled within the study areas (Figs 1, 2; Table 1). Altogether, more than 200 thin sections were examined by conventional microscopic petrographic methods. Cathodoluminescence (CL) petrography was carried out on selected samples using a Nuclide ELM–3R cold CL device operating at 10 kV. In order to distinguish between calcite, dolomite, and their ferroan variants, many of the thin sections were stained with a mixture of Alizarin Red-S and potassium ferricyanide as described by Dickson (1966). Folk's (1962) terminology was used for the crystal size characterization.

The geochemical analyses for major and trace elements of selected, polished, carbon-coated samples were carried out with an AMRAY 1830I/T6 scanning electron microscope (SEM) equipped with a MORAN energy-dispersive X-ray spectrometer. Dolomite was sampled for stable carbon and oxygen isotope analyses, using a hand-held microdrill with a 0.5-mm bit-head (28 samples). The carbonate powder was divided into two samples that were measured separately. The powder was analysed using the continuous flow technique with the H_3PO_4 digestion method (Rosenbaum and Sheppard 1986; Spötl and Vennemann 2003). $^{13}C/^{12}C$ and $^{18}O/^{16}O$ ratios of CO_2 generated by acid reaction were measured using a Thermo Finnigan Delta Plus XP continuous flow mass spectrometer equipped with an automated GasBench II. The results are expressed in the δ-notation on the Vienna Pee Dee Belemnite (V-PDB) standard, in parts per 1000 (‰). Duplicates of standards and samples were reproduced at better than ±0.15 and ±0.1 ‰, for oxygen and carbon isotopes, respectively.

Doubly polished thin sections (100 µm thick) of selected samples, which contain crystals suitable for measurements, were taken for fluid inclusion studies. Microthermometric measurements were performed on a Linkam FTIR 600 heating-freezing stage mounted on a polarised microscope. Standardization was carried out at –56.0, 0, and 374 °C on synthetic quartz-hosted H_2O and H_2O–CO_2 fluid inclusions. The accuracy of the measurements was 0.1 °C during heating experiments and 1 °C during freezing.

Dolomite petrography

Upper Triassic cherty dolomite

Thick-bedded (10–30 cm), cherty dolomite characterizes the succession in both studied areas. The dolomite contains grey or brown 5- to 10-cm-sized chert nodules and/or 1- to 2-cm-sized angular chert clasts (Fig. 3a). In the Buda Hills, alternations of dark and medium grey laminae were commonly observed in the upper part of the dolomite succession (Fig. 3b).

Under the microscope, various textural and fabric types of non-ferroan dolomite are encountered. The crystal size varies moderately or significantly in all samples. Finely to medium crystalline dolomite, consisting of crystals of ca. 10–150 µm in size, is volumetrically the most significant component in the succession (Fig. 4). Two textural types can be distinguished. In one of the types, closely packed subhedral–anhedral crystals occur, whereas in the other, medium-sized euhedral–subhedral crystals and fine crystals are heterogeneously distributed (Figs 4, 5). In both textural types, the crystals are either unzoned or have a turbid core and a limpid outer rim. Baroque dolomite, which is characterized by medium to coarse (up to 500 µm) anhedral crystals, is associated with finely to medium crystalline dolomite in variable amounts. The baroque crystals are commonly turbid, but coarser crystals have a turbid core and limpid rim. They show undulose extinction under crossed polars. The baroque crystals occur as a replacive phase as well as a pore-filling cement (Fig. 6). In the laminated dolomite, limpid baroque crystals are only observed as thin veins.

In the laminated dolomite, aphanocrystalline clots and peloids are encountered as minor components (Fig. 4a). Aggregates of tiny clots and the individual peloids are arranged into discontinuous bands and laminae. Very fine to fine crystals are encountered in the partially dolomitized limestone, which exhibits transitional features towards the overlying limestone. The tiny euhedral and subhedral dolomite crystals form clusters, or they are randomly scattered within the bioclastic–peloidal wackestone–packstone (Fig. 4c, d). The components and the depositional fabric gradually disappear where the dolomite crystals tend to be tightly intergrown. In many samples, the intercrystalline porosity within the sucrosic dolomite is occluded by brown organic matter (cf. Hetényi et al. 2004). Similar brown, residual organic matter is enriched along bed-parallel dissolution seams and stylolites as well as sub-vertical stylolites (Fig. 4b, d).

The pervasively dolomitized part of the formation is characterized by peculiar breccia fabric under the microscope. No preserved sedimentary components or sedimentary fabric can be recognized inside the clasts; thus, the dolomitization was fabric-destructive. The breccia fabric exhibits specific features. The breccia consists either solely of dolomite clasts, or solely of chert clasts, but both also co-occur. Well-defined as well as obscured brecciation is visible in the fabric where the boundary of clasts/mottles is relatively sharp or gradational, respectively (Figs 6, 7). In the case of the well-defined breccia, heterogeneously distributed mottles of fine to medium crystalline dolomite are cut across by irregular mottles of medium to coarse crystalline baroque dolomite (Fig. 6). Crosscutting relationships show that the formation of baroque crystals post-dates the finely to medium crystalline phases. In many cases, mottles consisting of crystals of different size are in direct contact; no groundmass (such as matrix or cement) surrounding each clast is encountered (Fig. 6a). The poorly defined breccia fabric is characterized by finely to medium crystalline mottles exhibiting either sharp or gradational boundary, or both together (Fig. 7). Strings consisting of medium-sized crystals commonly fan out forming a groundmass among the finer crystalline mottles (Fig. 7a). In a few samples, an enrichment of rhombohedral crystals within brecciated damage zone of microscale normal faults is observed (Fig. 5). All samples with breccia fabric are characterized by a gradually increasing crystal size from mottle to mottle that refers to a sequence of successive generations of replacive dolomite phases (Fig. 8). The final dolomite phase is a pore-filling, limpid baroque cement (Fig. 7c). Bed-parallel stylolites are occasionally encountered (Fig. 6a).

Under CL, the fine to medium, subhedral–anhedral crystals and the aphanocrystalline components show blotchy dull red luminescence (Fig. 5d). The rhombohedral medium-sized crystals display a core and growth zone of variously dull red luminescence. The medium and coarse, anhedral baroque crystals show dull red blotchy luminescence, or they have a blotchy core and a darker, faint red rim. Moreover, the subhedral baroque crystals may exhibit variously intense faint and dull red growth zones with a brighter red fine subzone. Luminescence of the baroque dolomite also revealed the formation sequence of the crystals as well as crosscutting dolomite veinlets (Fig. 9).

Breccia dolomite zones in the down-faulted basement of the basinal succession

A down-faulted block of the Middle Triassic platform carbonate (Budaörs Dolomite) forms the basement of the cherty dolomite in the Danube-East blocks. Three fabric types were observed. (1) Fabric-destructive, predominantly medium crystalline dolomite consists of closely packed subhedral–anhedral crystals 70–300 μm in size. The crystals are either inclusion-rich, or they have a turbid core and limpid rim. The majority of crystals show undulose extinction under crossed polars. This fabric type is volumetrically the most significant component in the studied succession. (2) The second type is characterized by a highly variable crystal size that ranges from aphanocrystalline to coarsely crystalline (ca. up to 400 μm). The aphanocrystals form clot-clusters or a dense groundmass in which finely or medium to coarsely crystalline mottles are embedded. However, an opposite pattern is locally observed; the medium crystalline dolomite involves finely crystalline stringers or clusters of peloids. (3) The third type is characterized by breccia fabric (Fig. 10). It was observed in some thin intervals. Two subtypes can be distinguished on the basis of the inner fabric of the clasts and crystal habits of embedding dolomite. In one of the subtypes (Fig. 10a), the clasts have similar fabrics to the two fabric types described above. The ratio of clasts and surrounding medium to coarse, anhedral baroque crystals is very low; many clasts are apparently floating in the embedding dolomite. In the other subtype (Fig. 10b), coarser crystalline clasts, occurring in a wide range of sizes, are embedded within dolomite micrite. The clasts consist of medium to coarse, anhedral baroque crystals which are either turbid, because of many solid inclusions, or limpid. Many of the limpid crystals are elongated and oriented perpendicular to the boundary surface of the turbid and limpid phases. These limpid crystals are truncated along the clast's boundary. Moreover, there is a subhedral, limpid baroque crystal generation, which shows straight crystal faces and which is attached onto the surface of breccia clasts.

Geochemical data

Major and trace element compositions

Homogeneous back-scattered electron images characterize the dolomite. Concentrations of trace elements are below the detection limit of the EDS detector that was used for this study.

Stable carbon and oxygen isotopes

The fine-scale heterogeneity and the size of the dolomite crystals inhibited their selective sampling. Only the fracture-filling baroque dolomite cement from large pores could be sampled and measured separately; otherwise, bulk rock samples were analysed (Fig. 11; Table 2). The $\delta^{13}C_{V\text{-}PDB}$ values of all samples are similar, ranging between 2.2 and 3.3 ‰. In contrast, the $\delta^{18}O_{V\text{-}PDB}$ values of coarse baroque dolomite (between –9.1 and –6.0 ‰) are much depleted in ^{18}O relative to those of bulk samples of finely to medium crystalline dolomite (between –1.3 and 2.1 ‰). The bulk rock values, representing all phases together, yielded a range from –5.4 to –1.3 ‰.

Fluid inclusion petrography and microthermometry

One suitable sample was analysed in order to obtain information on the temperature and the composition of dolomitizing fluid. Fluid inclusion studies were carried out on primary aqueous inclusions of the medium crystalline replacive subhedral dolomite crystals and the baroque dolomite cement. In the turbid core of the subhedral crystals, isometric primary fluid inclusions are also present from 1 to 5 μm in size. They are all monophase liquid inclusions, implying that the precipitation of the mineral occurred below 50 °C (Goldstein and Reynolds 1994).

Primary fluid inclusions are present in the core and along growth zones of the baroque dolomite crystals. They are 2–8 μm in size, and their shape is elongated or isometric and angular. The inclusions contain both liquid (L) and vapour (V) phases with visually determined L:V phase ratios of around 95:5 (Table 3; Fig. 12). Several secondary fluid inclusion assemblages were also observed along microfractures/cleavage planes. Microthermometry was carried out on the primary two-phase inclusions of baroque crystals. The inclusions were homogenized into liquid phase. The measured homogenization temperature values range between 72 and 108 °C (Fig. 12). Even though the entrapment temperature of the fluid could not be calculated, since no pressure correction was applied, the homogenization temperature values still provide a valid measure of the minimum entrapment temperature (Goldstein and Reynolds 1994). The vapour phase of the inclusions usually did not reappear during cooling down to room temperature or below; therefore, in most cases, it was not possible to measure the final melting temperature. The five obtained final melting temperatures range between –1.8 and –1.1 °C, which equals to a salinity range from 1.9 to 3.1 NaCl eq. wt%, assuming a NaCl–H2O system (FLINCOR software; Brown 1989).

Attempts to locate fluid inclusions suitable for microthermometric analysis from other collected samples were unsuccessful because many late-stage, thin fractures cut across the dolomite.

Discussion

Interpretation of the paragenetic sequence of the Upper Triassic cherty dolomite

Alteration of biogenic silica and silicification of the deposits are interpreted as being one of the first alteration processes. The non-dolomitized limestone succession is rich in radiolarians and sponge spicules (Haas et al. 1997a, 2000) that have been partly replaced by calcite and the mobilized silica impregnated the deposits in the relatively shallow burial diagenetic realm (e.g. Hesse 1990). Dolomite showing breccia fabric contains many angular chert clasts. These occur neither in the partially dolomitized limestone nor in the limestone upsection. Thus, they are probably not reworked sedimentary particles but fragments of chert nodules or chert laminae. These clasts were most likely formed in place during diagenesis, such as during or after the diagenetic alteration of silica, but before the formation of euhedral–subhedral dolomite rhombs, which appear among the clasts (Fig. 7a, b).

Fine to medium, subhedral–anhedral crystals are interpreted as being formed via a replacive process. The CL pattern indicates that the euhedral medium-sized crystals nucleated as replacive crystals and are enlarged successively by further replacement and in the latest phase as syntaxial overgrowth cement, similarly to the alteration stages described by Choquette and Hiatt (2008). Laminae of aphanocrystalline clot-clusters have been likely formed via shallow subsurface mineralization of bacterial biofilms (Riding 2000). Organogenic dolomite in hemipelagic deposits is characterized by a wide range in $\delta^{13}C$ values, reflecting enrichment of carbon incorporated into to the dolomite from different bacterial zones of organodiagenesis (e.g. Burns et al. 1988; Compton 1988; Mazzullo 2000; Meister et al. 2007). The aphanocrystal phase is minor in the studied samples. It cannot be determined whether the aphanocrystals formed via replacement of organogenic calcite precursor or they primarily precipitated as dolomite. A lack of carbon isotope shift towards negative values might be explained by the predominance of seawater-derived dissolved carbon in the pore fluid during the relatively short-term sulphate reduction (cf. Mazzullo 2000).

The primary monophase aqueous inclusions of the subhedral crystals indicate formation below 50 °C (Goldstein and Reynolds 1994). The oxygen isotope values between 2.1 and –1.3 ‰, measured from bulk rock samples of fine to medium crystalline dolomite, suggest formation at moderately wide temperature range (cf. Land 1983). The replacive baroque crystals were formed above 60 °C (Radke and Mathis 1980). Their formation temperature is approximated by minimum entrapment temperature of fluid inclusions (70 °C) that implies elevated temperature of the fluid compared to that of the replacive fine to medium crystals. The negative $\delta^{18}O$ values of the baroque crystals correlate with these results (cf. Land 1983). The combination of the isotopic data, the fluid inclusion data and the succession of dolomite phases observed indicates a dolomitization process by the same fluid at a different temperature rather than by various fluids of different compositions. This is supported by the observed uniform geochemical character of various-sized crystals. Accordingly, gradually coarser crystals replaced the precursor carbonate as a result of rising temperature followed by baroque cement precipitation (Figs 6, 8, 9).

Petrographic observations reveal that although the partially dolomitized limestone and the limestone upsection contain abundant bioclasts, none of them, except for some silicified ones, was preserved in the dolomite fabric (Fig. 4c). Thus, the dolomitization was fabric-destructive. Even if one assumes the retention of breccia fabric of the precursor limestone, there would be no explanation for the distinct crystal sizes of the adjacent clasts, the wide range of dolomite crystal size, and a lack of the surrounding matrix or cement (e.g. Fig. 6a). Bed-parallel stylolites in the dolomite indicate that dolomitization took place in intermediate burial diagenetic realm prior to the onset of chemical compaction (Fig. 6a).

Interpretation of the paragenetic sequence of the breccia dolomite in the down-faulted basement

The fabric types of the bedded platform dolomite in the Danube-East blocks resemble those of the Middle Triassic Budaörs Dolomite described in detail from the Buda Hills (Hips et al. 2015). A two-stage dolomitization model has been proposed for the Middle Triassic platform carbonate. Fine crystals with aphanocrystalline clot-clusters were formed during synsedimentary dolomitization, whereas medium and coarse crystals were formed during a thermal convection-induced dolomitization at intermediate burial depth.

Two different subtypes of breccia fabric indicate two stages of brecciation. The petrographic features of one of the breccia fabrics—characterized by two types of dolomite clasts floating in mainly coarsely crystalline dolomite—imply that rocks were at least partly dolomite by the time of brecciation (Fig. 10a). Additionally, a gradually increasing crystal size from clast-rich areas towards clast-free ones suggests that baroque crystals at first stage replaced the precursor $CaCO_3$ components, and then, the dolomite crystals subsequently precipitated as cement. These features, such as a replacive baroque dolomite phase overgrown by a cement phase, are observed within breccia clasts in other samples (Fig. 10b). The presence of cement phase indicates that fragmentation of the rocks was initiated via hydrofracturing, and the fluid was likely overpressured (Fig. 10a). The formation of coarse baroque dolomite suggests that the temperature of dolomitization was above 60 °C (Radke and Mathis 1980). The successive fracturing stages led to additional brecciation, where the features of breccia fabric imply friction-related fragmentation (Fig. 10b). Limpid crystals having straight crystal faces represent the latest-stage dolomite cement among the breccia clasts (Fig. 10b). In these later stages, the fluid was not overpressured.

Interpretation of organic matter data

The measured VR values required a basin-specific calibration because of co-occurrence of hydrogen-rich kerogens (comment by Vidó M.). The expected equivalent VR is ca. 0.5 % that is calculated from supressed VR (Vidó M., unpublished data). Correction was performed applying the method of Lo (1993) taking into consideration the elevated values of Rock–Eval HI, ranging between 200 and 500, and TOC content, ranging from 1 to 4 % (Hetényi et al. 2004). Accordingly, the maximum burial temperature of the succession might have been around 50–60 °C, estimated from the thermal maturity data (cf. Hunt 1996). A more reliable estimation would require further study and establishment of a basin-specific empirical VR-T model (cf. Chen et al. 2010). Dolomitization of the slope and basinal succession took place in the intermediate burial realm as revealed by post-dating chemical compaction. Accordingly, the deposits were further buried after the cessation of dolomitization when they reached the maximum burial temperature (as reflected by VR data). Forced maturation, as an indicator of upward circulating hot fluid (Davies and Smith Jr. 2006), is detected for organic matter within the dolomite succession since the small temperature difference caused by ca. 100-m-deeper burial of dolomite could not explain the observed difference in maturity of organic matter.

The proposed conceptual model of dolomitization

During the Triassic, the depositional area of the Transdanubian Range was a part of the shelf of the Neotethys Ocean (Haas et al. 1995). In the Carnian, during the spreading stage, down-faulting of the carbonate platform and development of extensional basins took place (Bertotti et al. 1993; Haas and Budai 1995). The hypothetical model for Carnian basin development and for geometry of displacement in the studied areas (Fig. 13) is based on the model by Wernicke and Burchfiel (1982), where a system of normal faults is characterized by a major fault with associated subsidiary faults and by a low-angle detachment fault with imbricate fault blocks in the hanging wall block (as shown in Fig. 4.4. in Twiss and Moores 2007). Different types of intraplatform half-graben arrangement occur (presented in Fig. 17.14. in Fossen

2011). The accommodation zone in the depositional area of the Buda Hills may contain horst or graben, and the connection between the two studied basins is unknown (Fig. 2). The setting, facies distribution and evolution of the Late Triassic basins were mainly tectonically controlled (Haas 1994, 2002; Haas et al. 2000). Dolomitization of relatively large dolomite bodies requires a fluid-dominated diagenetic system (e.g. Morrow 1990). The character of the hydrological setting, established following major earthquakes, has been found to be dependent on the style of fault displacement. Normal faults involve post-seismic compressional elastic rebound and displace large volumes of fluid from the crust (Muir-Wood and King 1993; Muir-Wood 1994). This model is generally accepted as a viable mechanism for hydrothermal fluid transport (Cox et al. 2001).

The majority of the Middle Triassic platform carbonate in the basement blocks, underlying the cherty dolomite, was already lithified and cemented before the onset of Late Triassic down-faulting (Hips et al. 2015). Therefore, the permeability of the rocks prior to the faulting and fracturing may have been rather reduced. The hydraulic brecciation and fracturing commenced within a distinct zone of the basement rocks (Fig. 10a). The overpressured dolomitizing fluid is thought to have been injected from the detachment zone (Fig. 13). The fluid flowed through the opened pathway, from the detachment zone through the platform carbonates, and reaching the overlying relatively soft sediment, its pressure was reduced to hydrostatic (e.g. Bjørlykke 2010). A progressing down-faulting of the solid basement blocks subsequently led to friction-related secondary brecciation (Fig. 10b).

In the slope and basinal deposits—due to the physical properties of soft sediment, namely its ductile response to tectonic stress—fractures do normally not stay open sufficiently long to transmit fluid (Bjørlykke 2010). However, if the fluid is hot, then a diffuse flow is maintained (Bjørlykke 1994, 2010). The permeability of faults is generally greater at depth where the rocks are brittle (Bjørlykke 1994), such as in the Middle Triassic platform carbonates. At shallower depth, the permeable basinal carbonate deposits facilitated lateral fluid migration away from the fault zones (cf. Frost et al. 2012). In the studied slope and basinal successions, at the early stage of dolomitization, the fluid diffusely ascended through the matrix porosity of the calcareous deposits, resulting in dispersed nucleation. Finely crystalline replacive alteration commenced around the nucleation centres. During the prolonged dolomitization process, deposits have been intermittently subjected to seismic shocks that led to segregation of solid dolomitized clasts within a semi-consolidated, porous calcareous ‘matrix’. The tectonically induced periodic brecciation facilitated the fluid flow within the porous calcareous ‘matrix’. Thus, the discontinuity surfaces were obscured due to the progression of the replacive dolomitization. At the late stage of dolomitization, the breccia fabric and fractures became more obvious within brittle, pervasively dolomitized deposits and cement crystals precipitated. Although the master fault itself between the footwall platform dolomite and the dolomitized basinal succession was not identified on the field, the progressing dolomitization in the course of penecontemporaneous tectonic activity is reflected in the dolomite fabrics (Fig. 13). The breccia fabric is neither inherited from the precursor carbonates nor formed via late-stage fragmentation of dolomite rocks, but was formed during the dolomitization process.

The thermal gradient of the fluid is considered as a potential driving force for its circulation (cf. Bjørlykke 1994, 2010). Pervasive dolomitization occurred in the vicinity of faults and in the stratigraphically lower part of the formations, which implies prolonged circulation. Breccia fabric with high variation in crystal size and precipitation of baroque crystals in the late stage of paragenetic sequence demonstrate this situation. The highest temperature of the dolomitizing fluid is expected here that is reflected most of all in the precipitation temperature of baroque cement crystals (70 °C). This was slightly higher than the maximum burial temperature of the succession (ca. 50–60 °C), estimated from the thermal maturity data. Forced maturation of the organic matter in the dolomitized interval is another support for hydrothermal dolomitization. Regardless of the driving force, the cooling of heated water can be expected towards the basin centre (Bethke and Marshak 1990; Bjørlykke 1994). Along the pathway, the fluid cooled via mixing with the marine-derived pore water of the deposits—fine to medium crystal phases and partial dolomitization upsection represent this situation.

Palaeontological data from the limestone succession deposited in the basin indicate that parts of the elevated blocks located among the extensional basins became subaerially exposed in the Rhaetian (Haas et al. 2000, 2010). Under humid climate, meteoric water lenses were established below surface within these blocks. Thus, deeply circulated freshwater could have mixed with fluid channelled along fault zones, which may explain the salinity data obtained from fluid inclusion analysis. The compilation of a comprehensive palaeogeographic scenario, including the location of master faults and the dimension of extensional basins, requires integration of biostratigraphic, sedimentological, and structural geological data. This would permit understanding the spatial distribution of dolomitization but is beyond the scope of the present study.

Conclusions

Dolomitized slope and basinal successions of the Late Triassic fault-controlled, extensional intraplatform basins were studied. Silicified carbonates were affected by a volumetrically significant dolomitization. The pervasive dolomitization of the lower part of the succession with extensively brecciated fabric implies the most active fluid circulation to be in the vicinity of faults. Upsection and laterally, the breccia fabric becomes obscured, and the dolomite is finer crystalline. Further upsection, dolomitization gradually diminished.

The basic features of the proposed conceptual model are as follows. Activation of normal fault zones facilitated the fluid transport. The dolomitizing fluid was expelled along those synsedimentary normal faults which controlled the development and subsidence of the basins in an extensional regime. The thermal gradient of the fluid is considered as a potential driving force for its circulation. The fluid was likely hydrothermal when it reached the semi-consolidated slope and basinal deposits but gradually cooled down via mixing with marine-derived pore fluids. Buoyancy-driven fluid flow is a plausible candidate for dolomitization in the intermediate burial realm that took place over a relatively large distance in a short time. Thus, the dolomitization is not restricted to the vicinity of faults.

In the basement block, the coarsely crystalline baroque dolomite, containing dolomite rock fragments and exhibiting extensively brecciated fabric, is interpreted as being the master fault zone itself (developed within the Middle Triassic platform carbonate; Danube-East blocks).

Acknowledgements

We thank Sándor Kele for geochemical measurements, Zsófia Poros and Bernadett Bajnóczi for the CL study, and Csaba Péró and Pál Pelikán for technical assistance. We are grateful to Mária Vidó and István Vető for their help in interpretation of organic matter data, and László Fodor for stimulating discussions on the structural evolution of the areas studied. We are very grateful to Henry Lieberman for grammatical corrections. We are thankful to journal reviewers, Paola Ronchi and Nereo Preto, for valuable comments and corrections. The first author is a grantee of the Bolyai János Scholarship. Funding for this project was provided by the Hungarian Scientific Research Fund, grant No. K 81296.

References

Baker ChE, Pawlewicz MJ (1986) The correlation of vitrinite reflectance with maximum temperature in humic organic matter. In: Buntebarth G, Stegena L (eds) Paleogeothermics, evaluation of geothermal conditions in the geological past. Lecture notes in Earth Sciences, vol 5. Springer, Berlin, pp 79–93

Báldi T (1986) Mid-Tertiary stratigraphy and paleogeographic evolution of Hungary. Akadémiai Kiadó, Budapest

Benkő K, Fodor L (2002) Structural geology near Csővár, Hungary. Földt Közl 132/2: 223–246 (in Hungarian with English absctract)

Bertotti G, Picotti V, Bernoulli D, Castellarin A (1993) From rifting to drifting: tectonic evolution of the South-Alpine upper crust from the Triassic to the Early Cretaceous. Sediment Geol 86:53–76

Bethke CM, Marshak S (1990) Brine migrations across North America the plate tectonics of groundwater. Annu Rev Earth Planet Sci 18:287–315

Bjørlykke K (1994) Fluid-flow processes and diagenesis in sedimentary basins. In: Parnell J (ed.) Geofluids: origin, migration and evolution of fluids in sedimentary basins, Special Publications vol 87. Geological Society, London, pp 127–40

Bjørlykke K (2010) Subsurface water and fluid flow in sedimentary basins. In: Bjørlykke K (ed) Petroleum geoscience, from sedimentary environments to rock physics, Elsevier, Berlin, pp 258–280

Brown PE (1989) FLINCOR; a microcomputer program for the reduction and investigation of fluid-inclusion data. Am Mineral 74/11–12:1390–1393

Burns SJ, Baker PA, Showers WJ (1988) The factors controlling the formation and chemistry of dolomite in organic-rich sediments: Miocene Drakes Bay Formation, California. In: Shukla V, Baker PA (eds) Sedimentology and geochemistry of dolostones, Special Publications vol 43. Society for Sedimentary Geology, Tulsa, pp 41–52

Chen Z, Issler DR, Stasiuk LD (2010) An empirical relation between present temperature and vitrinite reflectance for Cenozoic strata of the Beaufort-Mackenzie Basin, Canada. Geol Survey Can Open File 6407, Natural Resources Canada, Ottawa

Choquette PW, Hiatt EE (2008) Shallow-burial dolomite cement: a major component of many ancient sucrosic dolomites. Sedimentology 55:423–460

Compton JS (1988) Degree of supersaturation and precipitation of organogenic dolomite. Geology 16:318–321

Conlife J, Azmy K, Gleeson SA, Lavoie D (2010) Fluids associated with hydrothermal dolomitization in St. George Group, western Newfoundland, Canada. Geofluids 10:422–437

Cox SF, Knackstedt MA, Braun J (2001) Principles of structural control on permeability and fluid flow in hydrothermal systems. In: Richards JP, Tosda, RM (eds) Structural controls on ore genesis, Reviews vol 14. Society of Economic Geologists, Littleton, pp 1–24

Császár G, Haas J, Jocháné-Edelényi E (1984) A Dunántúli-középhegység bauxitföldtani térképe a kainozoós képződmények elhagyásával, M = 1:100 000. MÁFI, Budapest

Davies GR, Smith Jr. LB (2006) Structurally controlled hydrothermal dolomite reservoirs facies: An overview. AAPG Bull 90:1641–1690

Detre Cs, Dosztály L, Herman V (1988) The Upper Norian (Sevatian) fauna of Csővár. Ann Rep Hung Geol Inst 1986: 53–67 (in Hungarian)

Dickson JAD (1966) Carbonate identification and genesis as revealed by staining. J Sediment Petrol 36:491–505

Esteban M, Budai T, Juhász E, Lapointe Ph (2009) Alteration of Triassic carbonates in the Buda Mountains – a hydrothermal model. Cent Eur Geol 52/1:1–29

Fodor L, Magyari Á, Fogaras, A, Palotás K (1994) Tertiary tectonics and Late Paleogene sedimentation in the Buda Hills, Hungary. A new interpretation of the Buda Line. Földt Közl 124/2:129–305

Fodor L, Csontos L, Bada G, Győrfi I, Benkovics L (1999) Tertiary tectonic evolution of the Pannonian Basin system and neighbouring orogenesis: a new synthesis of palaeostress data. In: Durand B, Jolivet L, Horváth F, Séranne M (eds) The Mediterranean Basins: Tertiary Extension within the Alpine Orogen, Special Publications vol 156. Geological Society, London, pp 295–334

Folk RL (1962) Spectral subdivision of limestone types. In: Ham WE (ed) Classification of carbonate Rocks, vol 1. AAPG Memoir, Tulsa, pp 62–84

Fossen H (2011) Structural Geology. Cambridge University Press, Cambridge

Frost EL III, Budd DA, Kerans C (2012) Syndepositional deformation in a high-relief carbonate platform and its effect on early fluid-flow as revealed by dolomite patterns. J Sediment Res 82:913–932

Gale L (2010) Microfacies analysis of the Upper Triassic (Norian) "Bača Dolomite": early evolution of the western Slovenian Basin (eastern Southern Alps, western Slovenia). Geol Carpath 61/4: 293–308

Goldstein RH, Reynolds TJ (1994) Systematics of fluid inclusions in diagenetic minerals. short course no. 31 Society for Sedimentary Geology, Tulsa

Győri O, Poros Zs, Mindszenty A, Molnár F, Fodor L, Szabó R (2011) Diagenetic history of the Palaeogene carbonates, Buda Hills, Hungary. Földt Közl 141/4:341–361 (in Hungarian with English summary)

Haas J (1994) Carnian basin evolution in the Transdanubian Central Range, Hungary. Zbl Geol Paläont 11/12:1233–1252

Haas J (2002) Origin and evolution of Late Triassic backplatform and intraplatform basins in the Transdanubian Range, Hungary. Geol Carpath 53/3:159–178

Haas J, Budai T (1995) Upper Permian-Triassic facies zones in the Transdanubian Range. Riv Ital Paleont Stratigr 101/3:249–266

Haas J, Kovács S, Krystyn L, Lein R (1995) Significance of Late Permian–Triassic facies zones in terrain reconstruction in the Alpine–North Pannonian domain. Tectonophysics 242:19–40

Haas J, Tardi-Filácz E, Oravecz-Scheffer A, Góczán F, Dosztály L (1997a) Stratigraphy and sedimentology of Upper Triassic toe-of-slope and basin succession at Csővár, North Hungary. Acta Geol Hung 40/2:111–177

Haas J, Tardi-Filácz E, Góczán F, Oravecz-Scheffer A (1997b) Cretaceous insertations in Triassic(?) dolomites at Csővár, North Hungary. Acta Geol Hung 40/2:179–196

Haas J, Korpás L, Török Á, Dosztály L, Góczán F, Hámor-Vidó M, Oravecz-Scheffer A, Tardi-Filácz E (2000) Upper Triassic basin and slope facies in the Buda Mts. – Based on study of core drilling Vérhalom tér, Budapest. Földt Közl 103/3:371–421 (in Hungarian with English summary)

Haas J, Götz AE, Pálfy J (2010) Late Triassic to Early Jurassic paleogeography and eustatic history in the NW Tethyan realm: New insights from sedimentary and organic facies of the Csővár Basin (Hungary) Palaeogeogr Palaeoclimatol Palaeoecol 291:456-468

Haeri-Ardakani O, Al-Aasm I, Coniglio M (2013) Fracture mineralization and fluid flow evolution: an example from Ordovician–Devonian carbonates, southwestern Ontario, Canada. Geofluids 13:1–20

Hámor-Vidó M, Hufnagel H, Hetényi M (1998) Organic petrology and Rock-Eval pyrolysis of Triassic source rocks from the Transdanubian region Hungary, first description of organic constituents in sedimentary matter. 49th Annual Meeting of ICCP, Porto Portugal, Abstracts Book pp 59

Hesse R (1990) Origin of chert: diagenesis of biogenic siliceous sediments. In: Mcllreath IA, Morrow DW (eds) Diagenesis, reprint series no. 15 Geosci Canada, Ottawa/Ontario, pp 171–192

Hetényi M, Sajgó Cs, Vető I, Brukner-Wein A, Szántó Zs (2004) Organic matter in a low productivity anoxic intraplatform basin in the Triassic Tethys. Org Geochem 35:1201–1219

Hips K, Haas J, Poros Zs, Kele S, Budai T (2015) Dolomitization of Triassic microbial mat deposits (Hungary): Origin of microcrystalline dolomite. Sediment Geol 318:113–129

Hofmann K (1871) A Buda–Kovácsi hegység földtani viszonyai. MÁFI Évk 1:1–61

Hunt JM (1996) Petroleum geochemistry and geology, 2nd edn. W.H. Freeman, New York

Karádi V, Kozur HW (2013) Stratigraphically important Lower Norian conodonts from the Csővár borehole (Csv-1), Hungary – Comparision with the conodonts succession of the Norian GSSP candidate Pizzo Mondello (Sicily, Italy). In: Tanner LH, Spielmann JA, Lucas SG (eds) The Triassic system, vol 61. Bulletin New Mexico Museum Natural History Science, Albuquerque, pp 284–295

Kleb B, Benkovics L, Gálos M, Kertész P, Kocsányi-Kopecskó K, Marek I, Török Á (1993) Engineering geological survey of Rózsadomb area, Budapest, Hungary. Periodica Polytechnica – Civil Engineering, 37:261–303

Kozur H, Mock R (1991) New Middle Carnian and Rhaetian Conodonts from Hungary and the Alps. Stratigraphic importance and tectonic implications for the Buda Mountains and adjacent areas. Jb Geol B-A 134/2:271–297

Kozur H, Mostler H (1973) Mikrofaunistische Untersuchungen der Triasschollen im Raume Csővár, Ungarn. Verh Geol B-A 2:291–325

Land LS (1983) The application of stable isotopes to studies of the origin of dolomite and to problems of diagenesis of clastic sediments. In: Arthur MA, Anderson TF, Kaplan I.R, Veizer J, Land LS (eds) Stable isotopes in sedimentary geology, short course no. 10 Society of Sedimentary Geology, Tulsa, pp 4.1–4.22

Land LS (1985) The origin of massive dolomite. J Geol Educ 33:112–125

Lavoie D, Chi G (2010) Lower Paleozoic foreland basins in eastern Canada: tectono-thermal events recorded by faults, fluids and hydrothermal dolomites. Bull Can Petrol Geol 58/1:17–35

Lo HB (1993) Correction criteria for the suppression of vitrinite reflectance in hydrogen-rich kerogens: preliminary guidelines. Org Geochem 20:653-657

Machel HG (2004) Concepts and models of dolomitization: a critical reappraisal. In: Braithwaite CJR, Rizzi G, Darke G (eds) The geometry and petrogenesis of dolomite hydrocarbon reservoirs, Special Publications vol 235. Geological Society, London, pp 7–63

Machel H, Lonnee J (2002) Hydrothermal dolomite—a product of poor definition and imagination. Sediment Geol 152:163–171

Mazullo SJ (2000) Organogenic dolomitization in peritidal to deep-sea sediments. J Sediment Res 70/1:10–23

Meister P, McKenzie JA, Vasconcelos C, Bernasconi S, Frank M, Gutjahr M, Schrag DP (2007) Dolomite formation in the dynamic deep biosphere: results from the Peru Margin. Sedimentology 54:1007–1031

Morrow DW (1990) Dolomite – part 2: Dolomitization models and ancient dolostones, In: McIlreath IA, Morrow DW, (eds) Diagenesis, reprint series no. 4 Geoscience Canada, Ottawa/Onterio, pp 125–139

Muir-Wood R (1994) Earthquakes, strain-cycling and mobilization of fluids. In: Parnell J (ed) Geofluids: origin, migration and evolution of fluids in sedimentary basins, Special Publications vol 78.Geological Society, London, pp 85–98

Muir-Wood R, King GCP (1993) Hydrological signatures of earthquake strain. J Geophys Res 98B12: 22035–22068

Oliver J (1986) Fluids expelled tectonically from orogenic belts: their role in hydrocarbon migration and other geologic phenomena. Geology 14:99–102

Oravecz J (1963) Stratigraphic and facies problems of the Upper Triassic formations in the Transdanubian Range. Földt Közl 93/1:63–73

Poros Zs, Mindszenty A, Molnár F, Pironon J, Győri O, Ronchi P, Szekeres, Z (2012) Imprints of hydrocarbon-bearing basinal fluids on a karst system: mineralogical and fluid inclusion studies from the Buda Hills, Hungary. Int J Earth Sci 101:429–452

Qing H, Mountjoy EW (1992) Large-scale fluid flow int he Middle Devonian Presqu'ile barrier, Western Canada Sedimentary Basin. Geology 20:903–906

Qing H, Mountjoy EW (1994) Formation of coarsely crystalline, hydrothermal dolomite reservoirs int he Presqu'ile barrier, Western Canada Sedimentary Basin. AAPG Bull 78:55–77

Radke BM, Mathis RL (1980) On the formation and occurrence of saddle dolomite. J Sediment Petrol 50/4:1149–1168

Riding R (2000) Microbial carbonates: the geological records of calcified bacterial–algal mats and biofilms. Sedimentology 47/Suppl 1:179–214

Ronchi P, Masetti D, Tassan S, Camocino D (2012) Hydrothermal dolomitization in platform and basin successions during thrusting: a hydrocarbon reservoir analogue (Mesozoic of Venetian Southern Alps, Italy). Mar Petrol Geol 29:68–89

Rosenbaum J, Sheppard SMF (1986) An isotopic study of siderites, dolomites and ankerites at high temperatures. Geochem Cosmochim Acta 50:1147–1150

Rožič B, Kolar-Jurkovšek T, Šmuc A (2009) Late Triassic sedimentary evolution of Slovenian Basin (eastern Southern Alps): description and correlation of the Slatnik Formation. Facies 55/1: 137–155

Sasvári Á (2009) Middle Cretaceous (Aptian - Albian) shortening and tectonic burial of Gerecse Mountains, Transdanubian Range, Hungary. Dissertation, Eötvös University, Budapest

Smith Jr. LB, Davies GR (2006) Structurally controlled hydrothermal alteration of carbonate reservoirs: introduction. AAPG Bull 90:1635–1640

Spötl C, Vennemann TW (2003) Continuous-flow isotope ratio mass spectrometric analysis of carbonate minerals. Rapid Commun Mass Spectrom 17:1004–1006

Twiss RJ, Moores EM (2007) Structural geology, 2nd edn. WH Freeman and Company, New York

Wein Gy (1977) A Budai-hegység tektonikája (Tectonics of the Buda Hills). Hungarian Geological Institute Special Publication, Budapest (in Hungarian)

Wernicke B, Burchfiel BC (1982) Modes of extensional tectonics. J Struct Geol 4:104–115

Wilson MEJ, Evans MJ, Oxtoby NH, Satria Nas D, Donelly T, Thirlwall M (2007) Reservoir quality, textural evolution, and origin of fault-associated dolomites. AAPG Bull 91:1342–1344

Figure captions

Fig. 1 Two studied areas with the locations of the sampled sections. **a** Pre-Tertiary basement map of the Buda Hills (modified after Császár et al. 1984). **b** Map of the Csővár–Nézsa area without Quaternary formations (Benkő and Fodor 2002). *Inset map* showing Europe and Hungary with the location of maps

Fig. 2 Stratigraphic setting of the studied units (modified after Haas et al. 2000) with the position of the sampled sections. Probable locations of synsedimentary master faults are indicated

Fig. 3 a Thick-bedded dolomite containing abundant brown chert nodules (*arrow*); hammer for scale is 33 cm long. **b** Thick-bedded, laminated (*arrows*) dolomite. **a** Section 5, **b** Section 1

Fig. 4 Photomicrographs of the Upper Triassic dolomite showing dolomite textures. **a** Finely to medium crystalline dolomite with aphanocrystalline component which occurs in clot-clusters forming dissected lamina (*arrow*) and in scattered individual peloids. **b** Crystal size variation within finely to medium crystalline dolomite, the fabric of which typified by heterogeneous distribution of subhedral crystals. Remnant of organic matter (*brown*) occurs in intercrystalline porosity. **c** Partially dolomitized bioclastic–lithoclastic packstone with scattered tiny rhombohedral crystals (mainly in the *upper third* and *left bottom*; *arrows*). **d** Fine dolomite rhombs (10–20 μm; *arrows*) and residual organic matter (*brown*) along dissolution films in partially dolomitized limestone. **a** Section 3; **b** Section 6, at 242.3 m; **c**, **d** Section 7, at 87.1 m

Fig. 5 Photomicrographs of the Upper Triassic dolomite showing a typical texture. **a** Small-scale normal fault (*thick red arrow*) within thin layers of finely to medium crystalline dolomite. The displacement is 1 cm (not visible in the photomicrograph). Dolomite layers are either silicified (*brownish area*; *right* and *left*) or contains abundant residual organic matter (*black*; *middle top*). Calcite veinlets (*thin yellow arrows*) cut across the dolomite. **b** A detail of the damage zone of the fault shown in a. Among the chert and finely crystalline dolomite clasts, medium-sized euhedral–subhedral crystals developed post-dating the faulting. Silica (*brown*) impregnated the fault zone at a later diagenetic stage that post-dated the dolomitization. **c** A detail of the contact between the brecciated damage zone (*right*) and the laminated cherty dolomite (*left*) from the other part of the fault, not shown in **a**. **d** CL image of the components shown in **c**. *Right*: euhedral–subhedral medium-sized crystals show mottled dull *red* luminescence with *brighter*, *thin*, *outer* growth zone; silica among the dolomite crystals is *blue*. *Left*: predominantly fine crystals are mottled dull *red*;

chert among the dolomite crystals is non-luminescent; calcite veinlet is *bright orange* (*middle bottom*). Section 6, at 208.1 m

Fig. 6 Photomicrographs of the Upper Triassic dolomite showing the well-defined breccia fabric, crossed polars. **a** Mottles, with irregular boundaries, consist of crystals of various sizes. The crystal size ranges over a wide interval and shows a gradually increasing trend. A coarser crystalline mottle (*top right*) cuts across the boundary of fine and medium crystalline mottles. The interface between the mottles is occasionally serrated (bed-parallel stylolite; *arrow*). **b** Mottles, consisting of coarse, anhedral replacive and subhedral pore-filling cement crystals, are surrounded by fine to medium replacive crystals. The transition is commonly gradual between the mottles as shown by the gradually increasing crystal size, but sharp boundaries are also visible. Clayey detrital dolomite is the latest pore-occluding phase (*arrow*). Vertical silica veinlets cut across the dolomite crystals. Section 2

Fig. 7 Photomicrographs of the Upper Triassic dolomite showing the breccia fabric. **a** Variably sized dolomite and chert breccia clasts occur within *lighter grey* groundmass consisting of fine to medium, predominantly subhedral crystals. *Dark,* finer crystalline clasts have sharper boundaries, whereas mottles consisting of medium-sized crystals have more obscured ones. Faint hairlines (*light areas*; *arrow*) consisting of medium-sized crystals fan out downward forming a groundmass among the clasts. **b** Obscured boundary of finer crystalline mottles showing gradual transition towards the embedding medium crystalline groundmass (*arrows*). **c** Multiphase network exhibits gradually increasing crystal size, such as finely crystalline mottles appear as distinct clasts (*dark areas*) within a medium crystalline groundmass (*grey areas*). Limpid baroque dolomite cement (*white area*, *arrow*) precipitated within a fracture network post-dating the fine to medium replacive dolomite phases. Breccia fabric is more obvious in the *upper* part, whereas ghosts of clasts occur in the lower part. All these components are cut across by *light brown*, sub-vertical silica veins (*middle*). **d** The dolomite texture within a faint breccia fabric. Poorly defined clasts are typified by fine and medium, anhedral crystals, whereas dolomite micrite and medium-sized euhedral–subhedral crystals occur among them. Sharp boundaries (*thin yellow arrows*) as well as gradual transitions (*thick red arrows*) of clasts/mottles also occur. Larger clasts include many smaller, finely crystalline clasts (*yellow dotted circles*). **a**, **b** Section 6, at 230.9 m; **c** Section 5; **d** Section 6, at 247.6 m

Fig. 8 Photomicrographs of the Upper Triassic dolomite exhibiting the multiphase breccia fabric that is evidence of multi-stage progressing dolomitization. **a** *Numbers* mark the dolomite crystal phases of gradually increasing size, from dark, finely crystalline replacive dolomite through medium shade to the light, coarsely crystalline cement. The *numbered phases* represent the genetic order. Progressively changing character of the boundaries, from gradual to sharp, is typical. **b** A detail of fabric shown in **a**. The heterogeneous texture of clasts consists of predominantly fine crystals (phase 1). The *arrow* points to bands of slightly coarser crystals (phase 2, *lighter areas*). **c** A detail of fabric shown in **a**. A band of euhedral–subhedral crystals (phase 3) gradually disappears from *left* to *right* towards the area consisting predominantly of crystals of phase 2 (*arrow*). *Dark spots* are finely crystalline clasts (*yellow dotted circles*). **d** A detail of fabric shown in **a**, exhibiting faint brecciation; *brownish* medium-sized crystals (phase 3) occur among the poorly defined clasts of finer crystalline dolomite (phase 2; *arrow*). The wider fractures are occluded by coarse, limpid cement crystals (phase 4). *Dark spots* are finely crystalline clasts (*yellow dotted circle*). Section 7, at 535.8 m

Fig. 9 Photomicrographs of the Upper Triassic dolomite showing the fabric of baroque dolomite. **a** Medium-sized (*middle* and *right*) and coarse (*left*) baroque crystals. **b** CL image of the components shown in **a**. Medium-sized crystals are characterized by variously dull red growth bands where the final stage is *brighter red*, whereas the coarse crystals display dull *red* luminescence where the *brighter red* growth band appears in a relatively early stage of growth. A lack of the dark growth band in the coarser crystals suggests that their nucleation and growth post-date that of the medium-sized crystals. *Brighter red* luminescent dolomite phase surrounds the small, irregular mottles of *dull red* dolomite (*thick red arrow*) and brighter red luminescent veinlet (*thin yellow arrow*) cuts across the crystals. The non-luminescent components are pores (P). Section 7, at 540 m

Fig. 10 Photomicrographs of the Middle Triassic dolomite showing various types of the breccia fabric. **a** Various-sized clasts of aphanocrystalline dolomite (*dark*) and finely to medium crystalline fabric-destructive dolomite (*arrow*) are embedded within medium and coarsely crystalline baroque dolomite. The coarser baroque crystals are less inclusion-rich (*upper part*). **b** Multiphase breccia fabric with various-sized clasts consisting of turbid anhedral and coarser, less turbid anhedral–subhedral baroque cement crystals (the boundary of the two phases is marked by *thick red arrows*). Less turbid crystals (growth directions are shown by *thick red arrows*) are truncated at the edges of the breccia clasts. Limpid subhedral crystal (*middle*; *thin yellow arrow*) is overgrown on a clast. **a** Section 7, at 1122 m; **b** Section 7, at 1038 m

Fig. 11 Stable carbon and oxygen isotope cross-plot, samples from the Upper Triassic cherty dolomite

Fig. 12 Histogram of homogenization temperatures measured in primary two-phase (L-V) aqueous inclusions of baroque dolomite; sample from Section 7, at 540 m

Fig. 13 Schematic cross section of the studied Late Triassic extensional basins showing the conceptual model of dolomitization, not to scale. *(1)* Dolomitic limestone with very fine euhedral–subhedral crystals, fine to medium crystalline dolomite exhibiting lamination and faint breccia fabric were developed at relatively greater distance from the active fault and in the upper part of the Upper Triassic cherty dolomite succession. *(2)* Medium to coarsely crystalline dolomite displaying multiphase breccia fabric was developed closer to the active fault and in the lower part of the succession. *(3)* Multiphase breccia fabric occurs within distinct zones of the down-faulted basement block of the Middle Triassic platform dolomite

Table 1 List of the sampled sections

Table 2 Stable isotope values (V-PDB) from the Upper Triassic cherty dolomite

Table 3 Homogenization temperature values of primary fluid inclusions from baroque dolomite; Section 7, at 540 m

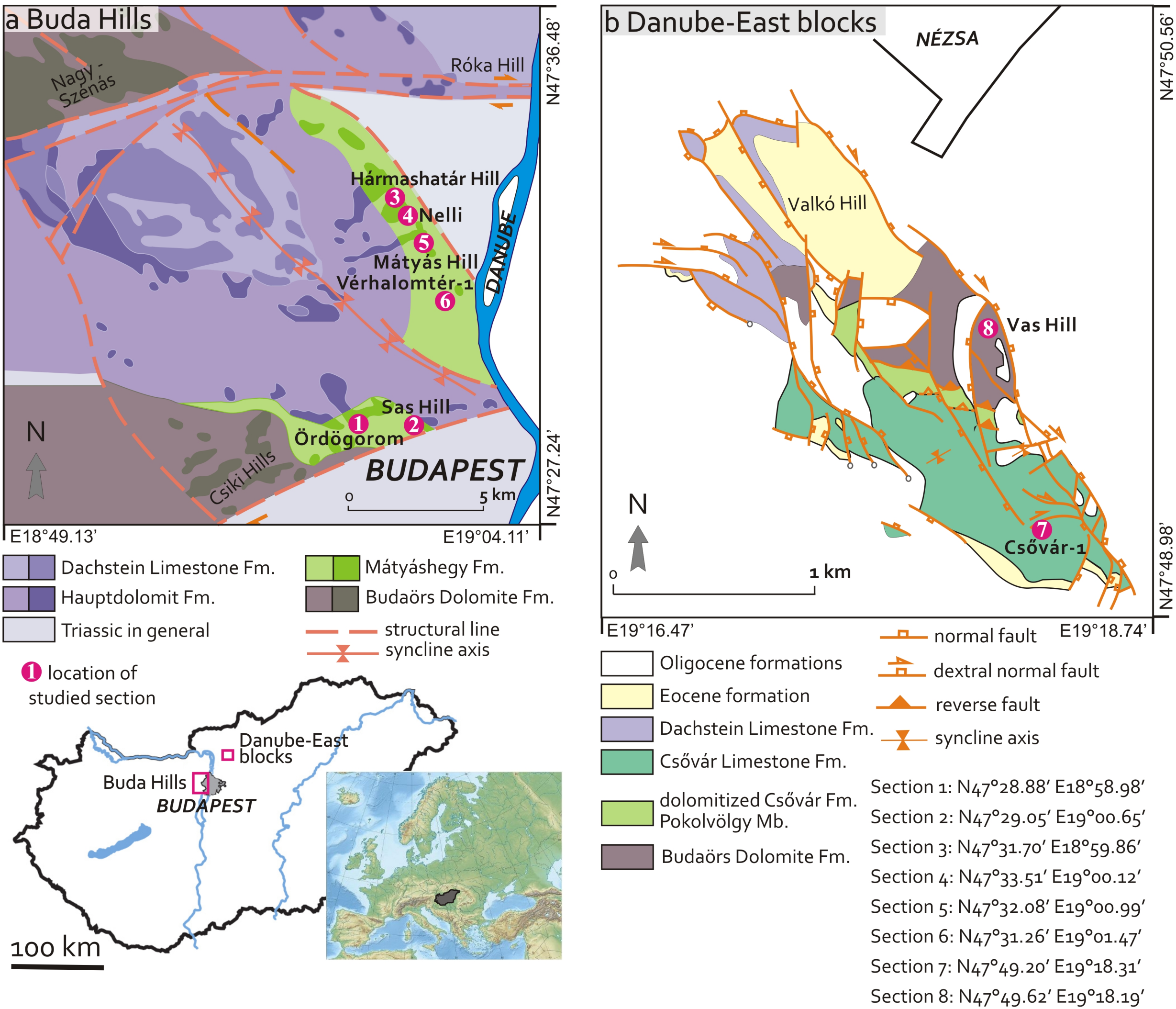
a Buda Hills
Nagy - Szénás
Róka Hill
Hármashatár Hill
3
4 Nelli
5
Mátyás Hill
Vérhalomtér-1
6
DANUBE
Sas Hill
1
2
Ördögorom
BUDAPEST
Csiki Hills
N
0
5 km
N47°36.48'
N47°27.24'
E18°49.13'
E19°04.11'
Dachstein Limestone Fm.
Hauptdolomit Fm.
Triassic in general
Mátyáshegy Fm.
Budaörs Dolomite Fm.
structural line
syncline axis
1 location of studied section
Danube-East blocks
Buda Hills
BUDAPEST
100 km
b Danube-East blocks
NÉZSA
Valkó Hill
8 Vas Hill
7
Csővár-1
N
0
1 km
N47°50.56'
N47°48.98'
E19°16.47'
E19°18.74'
normal fault
dextral normal fault
reverse fault
syncline axis
Oligocene formations
Eocene formation
Dachstein Limestone Fm.
Csővár Limestone Fm.
dolomitized Csővár Fm. Pokolvölgy Mb.
Budaörs Dolomite Fm.
Section 1: N47°28.88' E18°58.98'
Section 2: N47°29.05' E19°00.65'
Section 3: N47°31.70' E18°59.86'
Section 4: N47°33.51' E19°00.12'
Section 5: N47°32.08' E19°00.99'
Section 6: N47°31.26' E19°01.47'
Section 7: N47°49.20' E19°18.31'
Section 8: N47°49.62' E19°18.19'

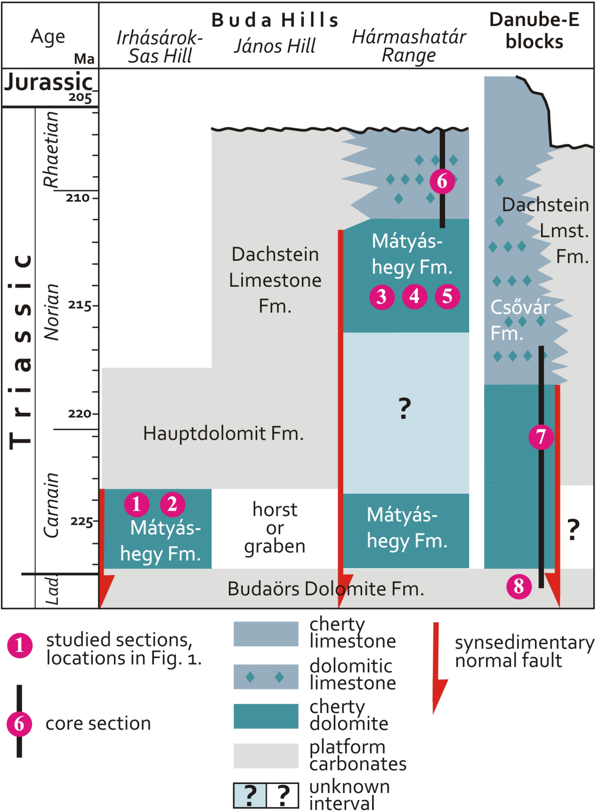

Age
Ma
Buda Hills
Irhásárok-Sas Hill
János Hill
Hármashatár Range
Danube-E blocks
Jurassic
205
Triassic
Rhaetian
210
Norian
215
220
Carnain
225
Lad.
Dachstein Limestone Fm.
Mátyás-hegy Fm.
Dachstein Lmst. Fm.
Csővár Fm.
?
Hauptdolomit Fm.
horst or graben
Budaörs Dolomite Fm.
1
2
3
4
5
6
7
8
studied sections, locations in Fig. 1.
core section
cherty limestone
dolomitic limestone
cherty dolomite
platform carbonates
unknown interval
synsedimentary normal fault

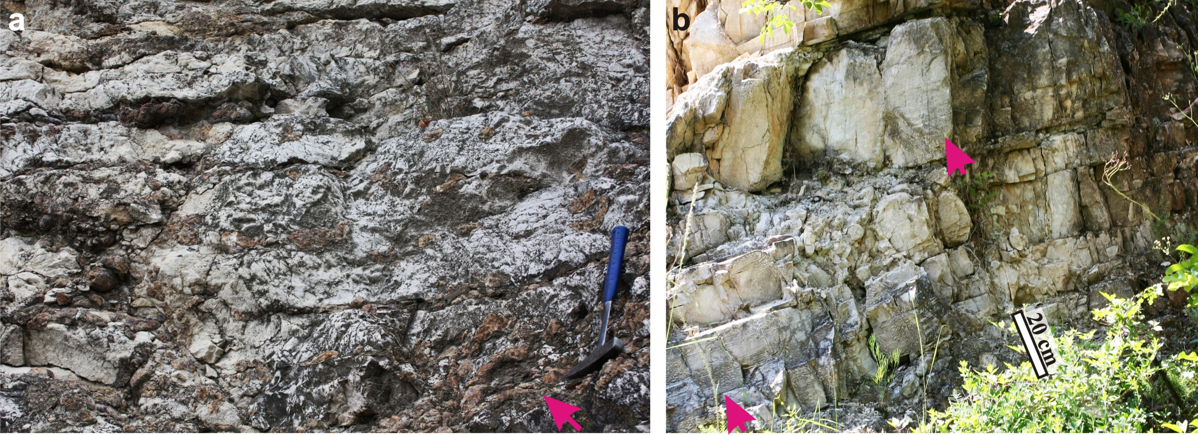
a
b
20 cm

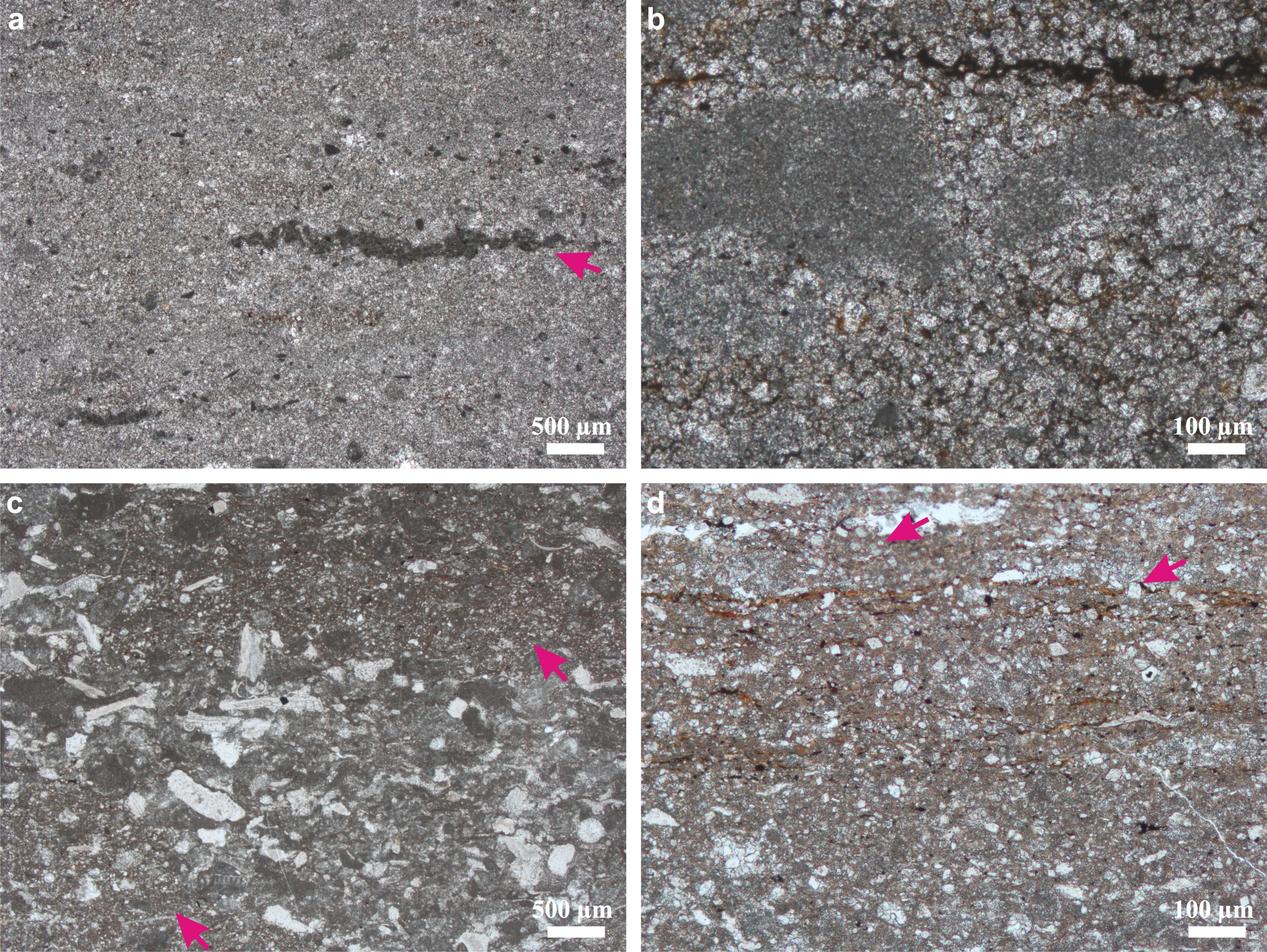
a
500 µm
b
100 µm
c
500 µm
d
100 µm

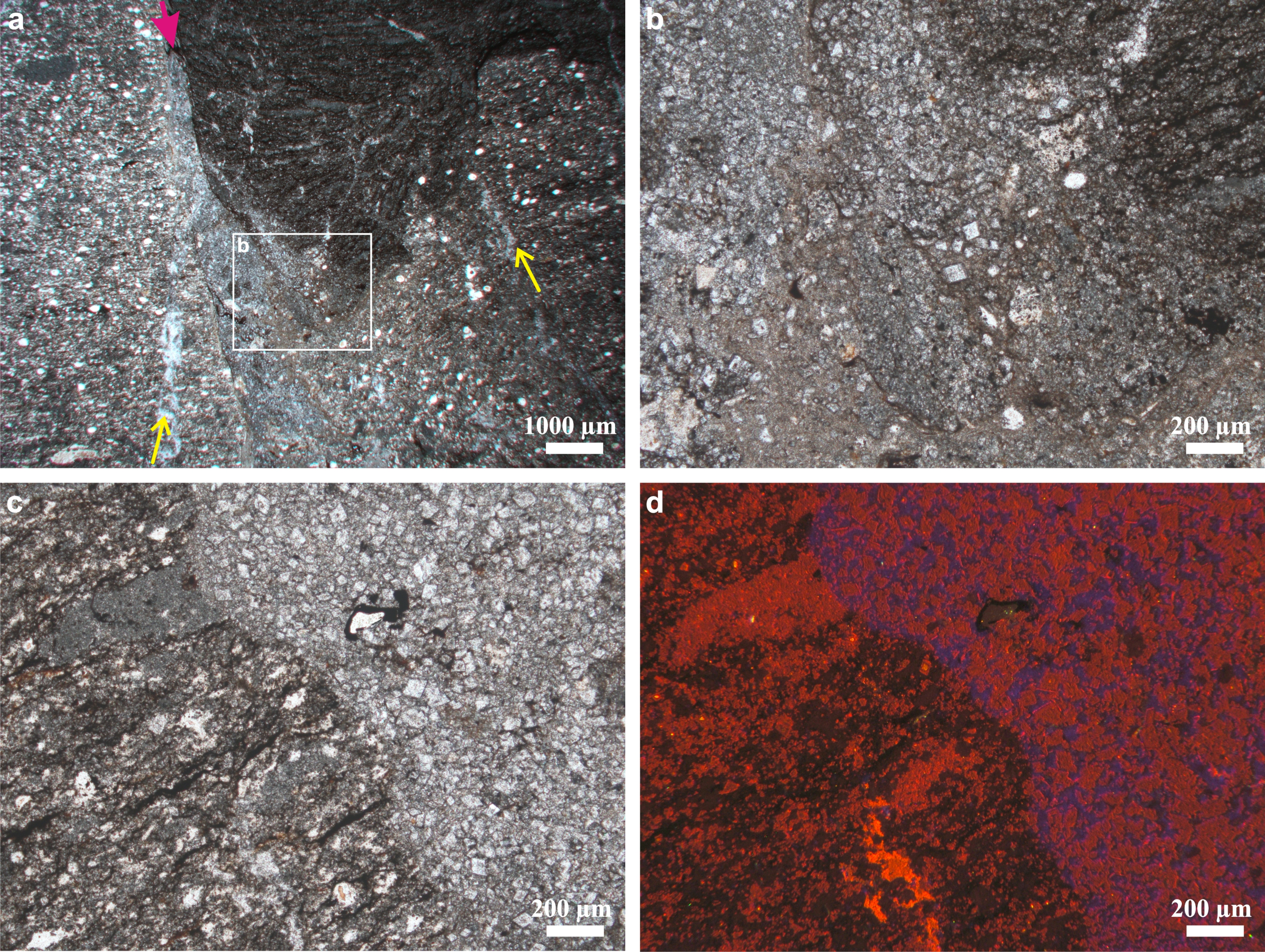
a
b
1000 μm
b
200 μm
c
200 μm
d
200 μm

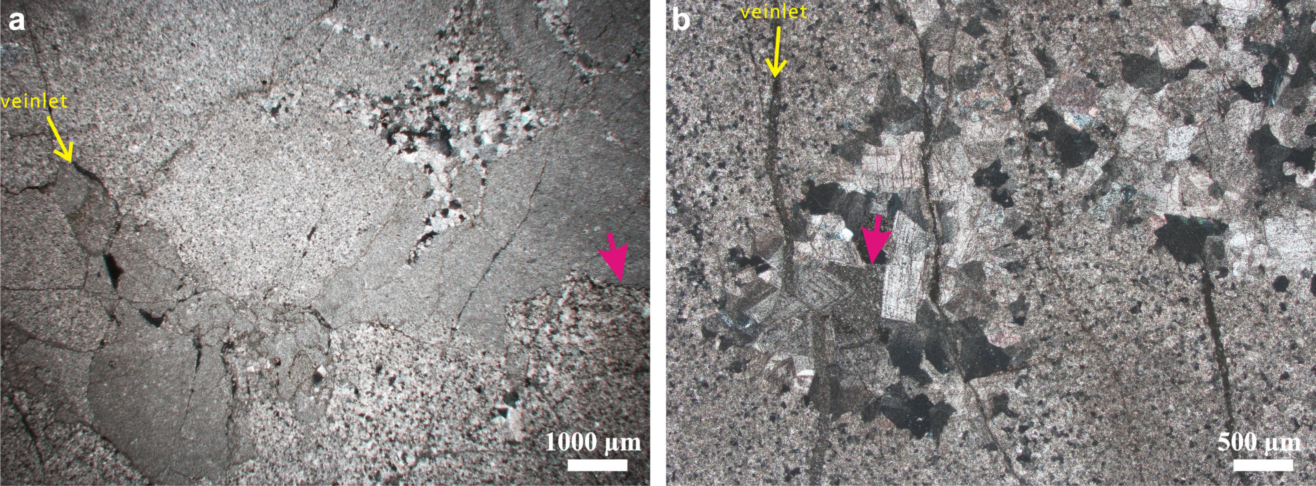
a
veinlet
1000 µm
b
veinlet
500 µm

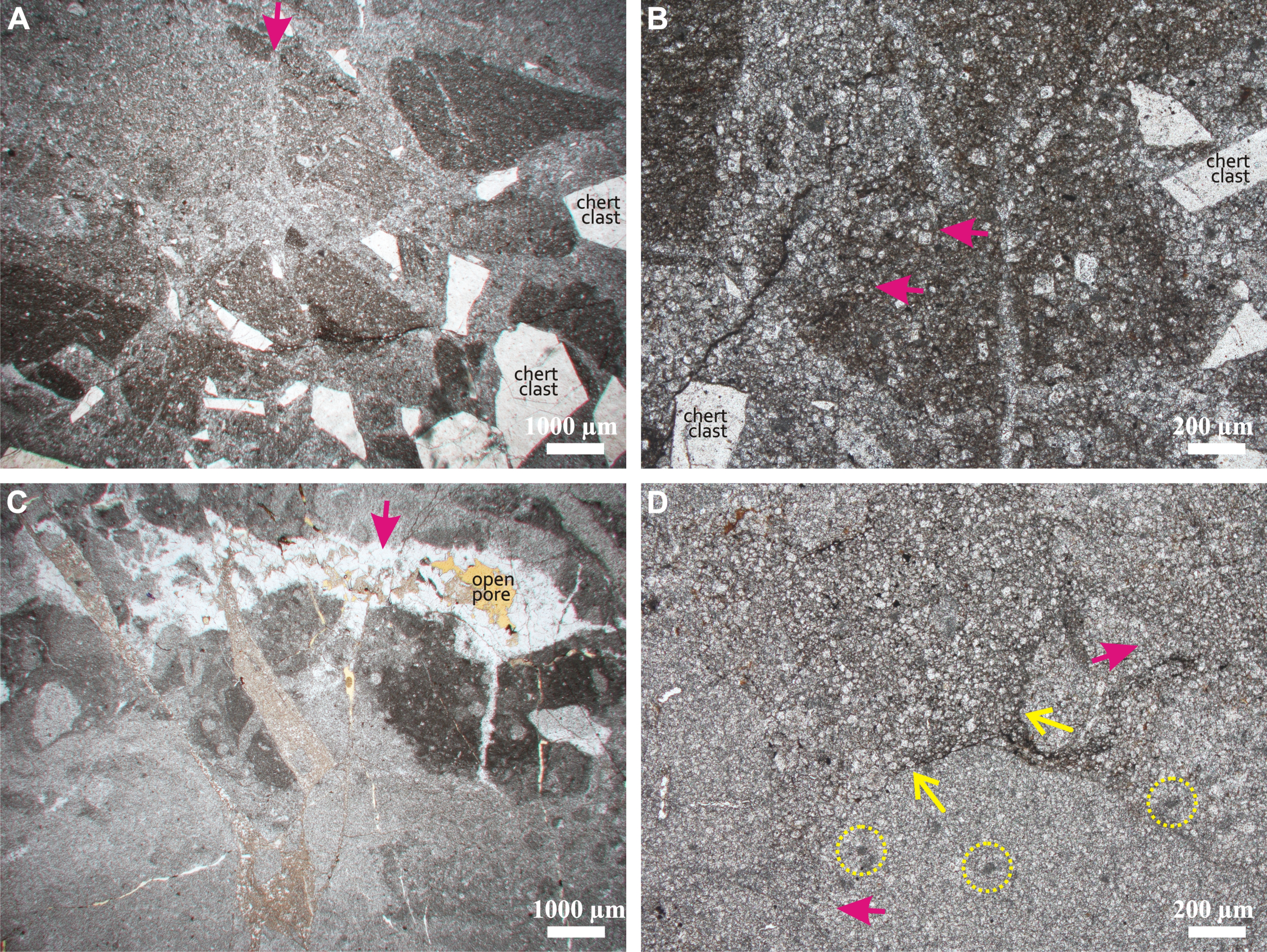
A
chert clast
chert clast
1000 µm
B
chert clast
chert clast
200 µm
C
open pore
1000 µm
D
200 µm

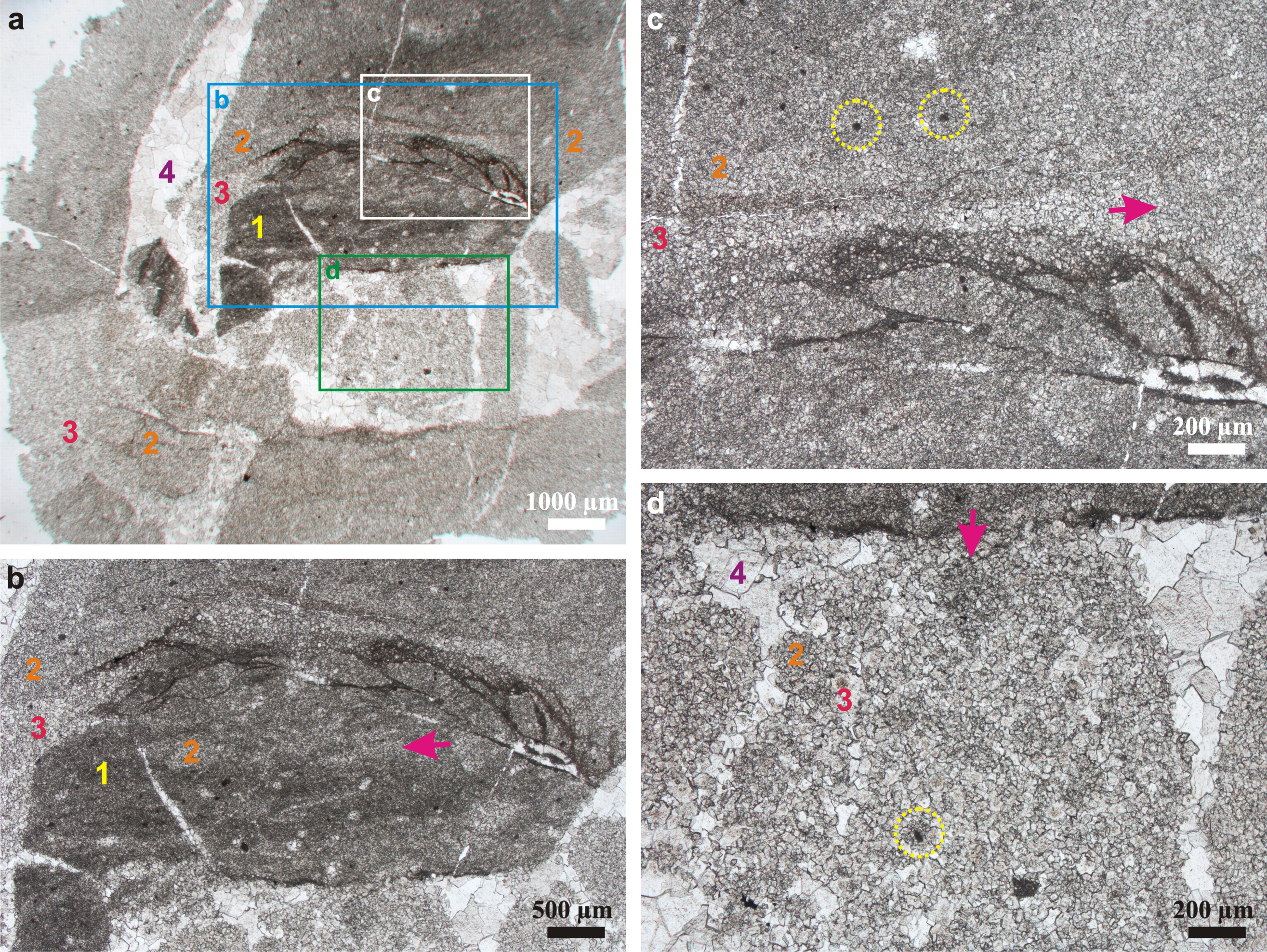
a
b
c
d
2
4
3
1
2
3
2
1000 µm
c
2
3
200 µm
b
2
3
1
2
500 µm
d
4
2
3
200 µm

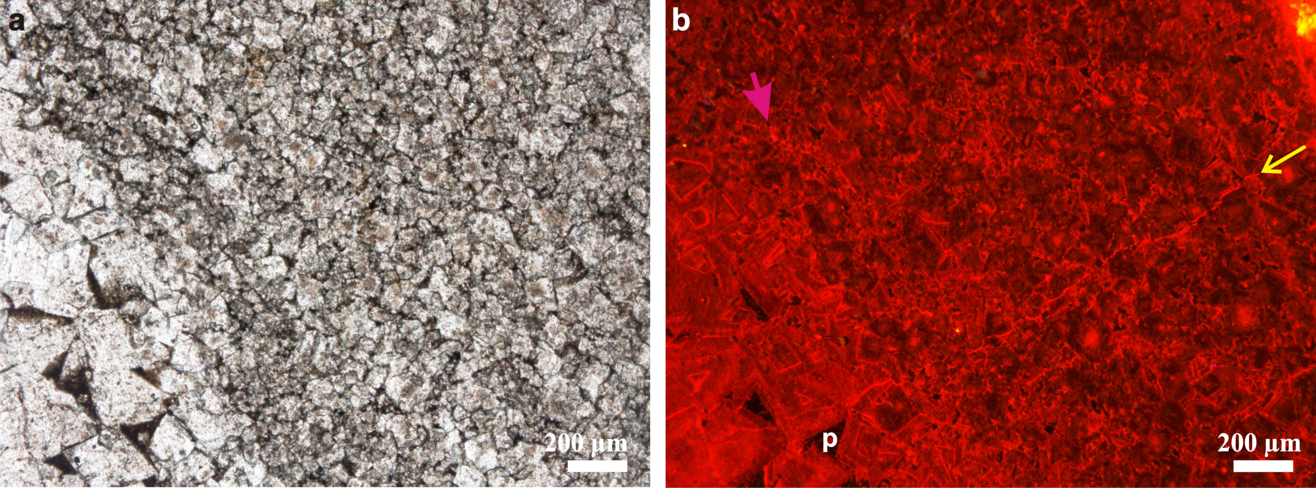
a
200 µm
b
p
200 µm

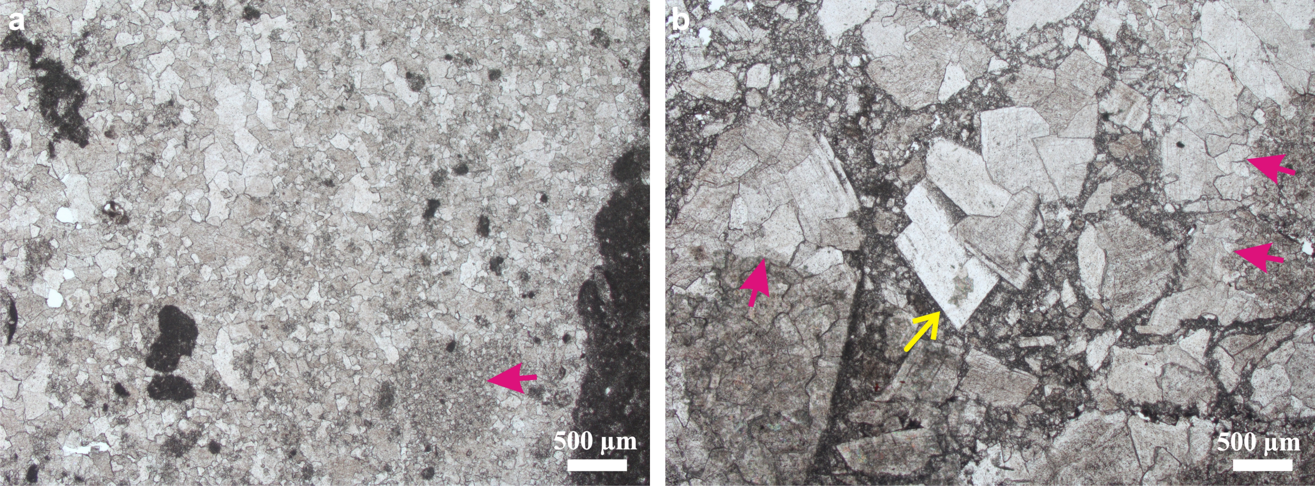
a
500 µm
b
500 µm

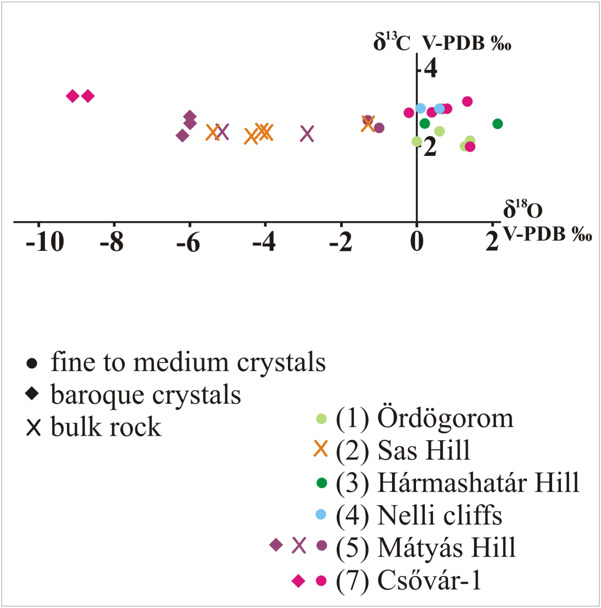

δ13C V-PDB ‰
4
2
δ18O V-PDB ‰
-10
-8
-6
-4
-2
0
2
fine to medium crystals
baroque crystals
bulk rock
(1) Ördögorom
(2) Sas Hill
(3) Hármashatár Hill
(4) Nelli cliffs
(5) Mátyás Hill
(7) Csővár-1

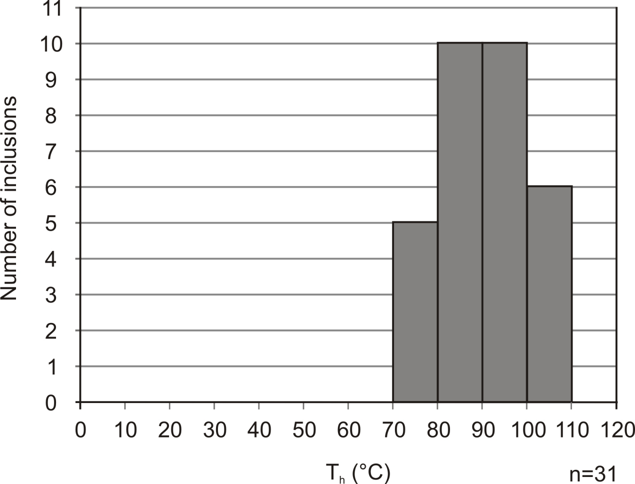
Number of inclusions
0
1
2
3
4
5
6
7
8
9
10
11
0
10
20
30
40
50
60
70
80
90
100
110
120
T_h (°C)
n=31

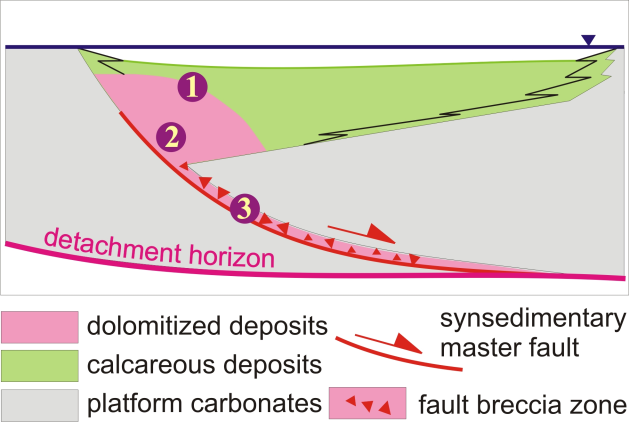
1
2
3
detachment horizon
dolomitized deposits
calcareous deposits
platform carbonates
synsedimentary
master fault
fault breccia zone

Section	Location	Formation	Thickness (m)	Lithology	Samples
1	Ördögorom, abandoned quarry	Mátyáshegy Fm.	5	Laminated dolomite	2
2	Sas Hill, road cut in the Meredek street	Mátyáshegy Fm.	5	Thick-bedded, cherty dolomite	4
3	Hármashatár Hill, outcrops at the top of the hill	Mátyáshegy Fm.	30	Laminated dolomite	2
4	Hármashatár Hill, Nelli cliffs	Mátyáshegy Fm.	10	Thick-bedded, cherty dolomite	2
5	Mátyás Hill, abandoned quarry	Mátyáshegy Fm.	20	Thick-bedded, cherty dolomite	6
6	Vérhalom-1 core section	Mátyáshegy Fm.	54	Limestone	36
			84	Thin-bedded alternation of dolomitic limestone, dolomite and chert	60
			52	Laminated dolomite	50
7	Csővár-1 core section	Csővár Fm.	522	Alternation of dolomitic limestone, cherty limestone and limestone	10
			100	Cherty dolomite	87
		Budaörs Fm. (basement block)	430	Dolomite	50
8	Vass Hill, cliff at the top	Budaörs Fm. (basement block)	10	Dolomite	5

Section	Dolomite fabric	$\delta^{13}C$ (‰)	$\delta^{18}O$ (‰)
1	fine to medium crystals	2.1	1.4
1	fine to medium crystals	2.0	1.3
1	fine to medium crystals	2.4	0.5
1	fine to medium crystals	2.1	0.0
2	fine to coarse crystals	2.6	-1.3
2	fine to coarse crystals	2.4	-4.0
2	fine to coarse crystals	2.4	-4.1
2	fine to coarse crystals	2.3	-4.4
2	fine to coarse crystals	2.4	-5.4
3	fine to medium crystals	2.6	0.2
3	fine to medium crystals	2.6	2.1
4	fine to medium crystals	3.0	0.1
4	fine to medium crystals	3.0	0.5
5	fine to medium crystals	2.5	-1.0
5	fine to medium crystals	2.7	-1.3
5	medium to coarse crystals	2.3	-2.9
5	medium to coarse crystals	2.4	-5.2
5	fine to coarse crystals	2.5	-6.0
5	fine to coarse crystals	2.6	-6.0
5	fine to coarse crystals	2.3	-6.2
7	fine to medium crystals	2.0	1.4
7	fine to medium crystals	3.2	1.3
7	fine to medium crystals	3.0	0.8
7	fine to medium crystals	3.0	0.7
7	fine to medium crystals	2.9	0.4
7	fine to medium crystals	2.9	-0.2
7	coarse dolomite cement	3.3	-8.7
7	coarse dolomite cement	3.3	-9.1

Grain	FI	Th (L-V) L (°C)	Tm (ice) (°C)	Salinity eq. NaCl (wt %)
119fz1/1	1	92		
119fz1/2	1	88		
119fz1/3	1	101		
	2	89		
119fz1/4	1	85		
119fz1/5	1	83	-1.1	1.9
119fz1/7	1	82		
119fz1/9	1	87		
119fz1/10	1	72		
119fz1/11	1	108		
	2	103		
119fz1/12	1	92	-1.8	3.06
119fz1/13	1	88		
119fz1/16	1	76		
119fz1/19	1	88		
	2	80	-1.4	2.4
	3	80	-1.4	2,4
119fz1/21	1	89		
119fz2/3	1	95		
119fz2/6	1	106		
119fz2/7	1	100	-1.6	2.73
	2	103		
	3	97		
119fz2/8	1	98		
119fz2/9	1	100		
119fz2/10	1	97		
	2	93		
119fz2/13	2	98		
119fz2/15	1	103		
119fz2/16	1	87		
119fz2/17	1	77		